ACS OMEGA

http://pubs.acs.org/journal/acsodf

Article

Cellulose Regeneration in Imidazolium-Based Ionic Liquids and Antisolvent Mixtures: A Density Functional Theory Study

Lanlan Fu, Zhaoyang Ju,* Mengting Yu, Huaying Luo, Cheng Zhang, Ximing Zhang, Haixiang Cheng, Minjia Zheng, Lu Jin, and Chengsheng Ge*

Cite This: *ACS Omega* 2022, 7, 42170−42180

Read Online

ACCESS | Metrics & More | Article Recommendations | Supporting Information

ABSTRACT: Cellulose can be dissolved in ionic liquids (ILs), and it can be recovered by adding antisolvent such as water or alcohol. In addition, the regenerated cellulose can be used for textiles, degradable membranes, hydrogels/aerogels, *etc.* However, the regenerated mechanism of cellulose remains ambiguous. In this work, density functional theory (DFT) calculation is reported for the cellulose regeneration from a cellulose/1-*n*-butyl-3-methylimidazolium acetate (BmimOAc)/water mixture. To investigate the microscopic effects of the antisolvents, we analyzed the structures and H-bonds of BmimOAc-$n$$H_2O$ and cellobiose-ILs-$n$$H_2O$ (n = 0−6) clusters. It can be found that when $n \geq 5$ in the BmimOAc-$n$$H_2O$ clusters, the solvent-separated ion pairs (SIPs) play a dominant position in the system. With the increasing numbers of water molecules, the cation−anion interaction can be separated by water to reduce the effects of ILs on cellulose dissolution. Furthermore, the BmimOAc-$n$$H_2O$ and cellobiose-ILs (n = 0−6) clusters tend to be a more stable structure with high hydration in an aqueous solution. When the water molecules were added to the system, H-bonds can be formed among H_2O, the hydroxyl of cellulose, and the oxygen of OAc. Therefore, the interactions between cellulose and ILs will be decreased to promote cellulose regeneration. This work would provide some help to understand the mechanism of cellulose regeneration from the view of theoretical calculation.

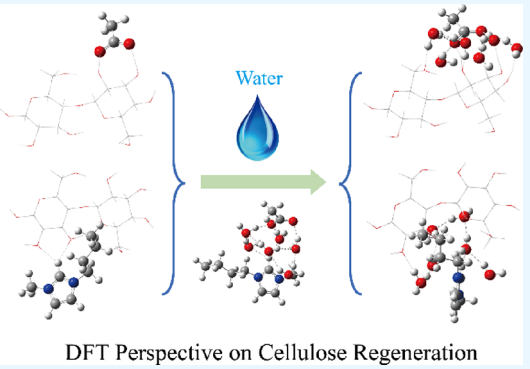

DFT Perspective on Cellulose Regeneration

1. INTRODUCTION

Renewable and green resources have been rapidly developed to face the global challenge of energy crisis and the environment in the past few years. Cellulose is one of the richest biopolymers in the world with an estimated annual yield of more than 10^{12} tons.[1] As a cheap and rich raw material, cellulose can be broadly used in paper, paints, textiles, and pharmaceutical compounds.[2,3] The utilization of renewable cellulose has shown great promise for the future, and it can be used as an appropriate feedstock for biofuel and bioproducts.[4,5]

Cellulose is a linear condensation polymer that connects the D-glucose units through the β-1,4-glycosidic bonds, with degrees of polymerization (DP) from 100 to 20,000 depending on the source.[6,7] Adjacent glucose molecules are connected by hydrogen bonds (H-bonds) and van der Waals forces, resulting in a parallel structure and crystal structure.[8,9] H-bonds can be formed with the hydroxyl groups of the chains, and these lead to structural robustness with strong mechanical strength. Therefore, cellulose cannot be dissolved in water and general organic solvents, such as ethanol, ether, acetone, *etc.* Ionic liquids (ILs) are organic molten salts with melting points below 100 °C, and they have been considered as green sustainable solvents for the dissolution of cellulose.[10,11] There are some special physicochemical characteristics for ILs, such as negligible vapor pressure, nonflammability, wide liquid range, and strong thermal stability. These have led ILs to be widely used in many fields, including catalysis, extraction, electrochemistry, organic synthesis, *etc.*[12,13] In 2002, Rogers and co-workers reported the use of ILs as cellulose solvents for both physical cellulose dissolution and regeneration, opening up a new class of solvents to the cellulose research community.[14] Uto *et al.* studied the dissolution of cellulose in imidazolium-based ILs by molecular dynamics (MD) simulation, and they proposed that the solubility of cellulose is closely related to the number of intermolecular H-bonds in cellulose crystals, and both anions and cations in ILs can promote the breakage of H-bonds.[15] So far, approximately 300 kinds of ILs have been tested experimentally for dissolving lignocellulosic biomass.[16−18] After the cellulose is dissolved in ILs, it can be regenerated from the cellulose/ILs/antisolvent

Received: August 2, 2022
Accepted: October 25, 2022
Published: November 7, 2022

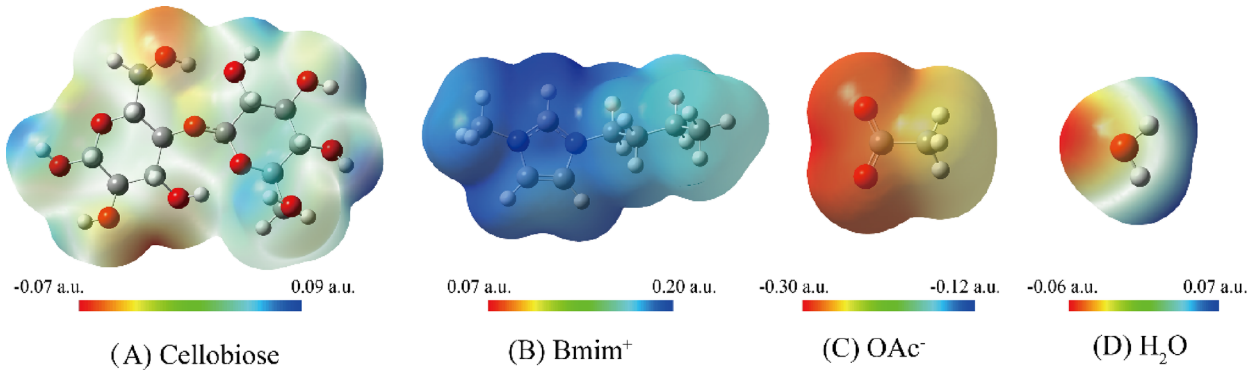

Figure 1. Electrostatic potential surface of optimized (a) cellobiose, (b) Bmim, (c) OAc, and (d) H_2O (isovalue = 0.0004 a.u.).

for further treatment. However, the study of cellulose regeneration is far less than dissolution.

Regenerated cellulose by coagulation with antisolvent is an important pathway for the industrialization of cellulose materials. Regenerated cellulose has high crystallinity and smoother surface morphology and does not generate static electricity easily, making it ideal for clothes. The stretching property can greatly improve the crystallinity and orientation of fibers with high thermal stability.[19,20] Zhu *et al.* used sol−gel technology to prepare regenerated cellulose membranes, and the mechanical properties of regenerated cellulose membranes are significantly improved due to the formation of H-bonds.[21] Hauru *et al.* measured the threshold of cellulose regeneration by water using nephelometry and rheometry and found that Kamlet−Taft (KT) parameters remain almost constant at 20−100 °C, even at different water contents.[22] At present, most of the research on cellulose is focused on the yield and properties of cellulose regeneration. However, the microscopic mechanism of cellulose regeneration, the interactions between ILs and antisolvents, and the roles of antisolvent in cellulose regeneration have not been revealed yet.

With the rapid development of computer technology, computational modeling methods such as MD, ab initio, and density functional theory (DFT) calculations have been successfully applied to the transformation mechanism of lignocellulose in ionic liquids.[23−25] Payal *et al.* investigated the structures and dissolution mechanism for cellobiose and xylan in ILs by DFT calculations in the gas phase and implicit and explicit solvents, and proposed inter-/intramolecular H-bonds play an important role in the dissolution.[26] Zhao *et al.* reported the effect of cosolvents on the solubility of cellulose in imidazolium-based IL systems by influencing H-bond interactions using MD and quantum chemistry calculations.[27] Liu *et al.* reported binary and ternary mixtures of 1-ethyl-3-methylimidazolium acetate with water and a cellulose oligomer by MD simulations, and they proposed that the introduction of water changes the structural organization of ILs and disrupts the interactions between ILs and cellulose.[28] The regeneration mechanism of cellulose in the cellulose/IL mixture has important theoretical guiding significance for the selection of suitable antisolvents. As one kind of efficient IL for cellulose dissolution and regeneration, 1-butyl-3-methylimidazolium acetate (BmimOAc) has been successfully used in the utilization of lignocellulose.[29,30] However, the regeneration mechanism of cellulose in the BmimOAc and water mixed system remains ambiguous.

In this work, as a common IL in the dissolution of cellulose, BmimOAc is used to study the effects of water on the regeneration of cellulose. Due to the limited computational capacity by using DFT calculations, cellulose is modeled by cellobiose, which consists of glucopyranose units by covalent β-1,4-glycosidic bonds.[31,32] We mainly study the roles of water in the BmimOAc and cellulose-ILs system. A series of BmimOAc-$n$$H_2O$ ($0 \leq n \leq 6$) clusters were optimized to reveal the roles of water in ILs. The geometries, interaction energies, and H-bonds of ILs/water clusters were analyzed. To further reveal the regeneration mechanism of cellulose, a series of cellobiose-OAc-$n$$H_2O$ and cellobiose-Bmim-$n$$H_2O$ ($0 \leq n \leq 6$) complexes were analyzed by the geometries and interaction energies. In addition, the quantum theory of atom in molecules (AIM) and independent gradient model based on Hirshfeld partition (IGMH) analysis were used to distinguish the bonding properties of the cellobiose-ILs-$n$$H_2O$ conformations. The regeneration mechanism of cellulose in BmimOAc/water mixtures was preliminarily proposed by DFT calculations, and the microscopic mechanism of cellulose regeneration can provide a certain theoretical basis for the utilization of cellulose.

2. COMPUTATIONAL METHODS

In this work, the geometry optimizations of the BmimOAc-$n$$H_2O$ (n = 0−6) clusters and cellobiose-ILs- $n$$H_2O$ ($0 \leq n \leq 6$) were performed using the DFT method with the M06-2X-D3 hybrid exchange-correlation functional and the def2SVP basis set as implemented in the Gaussian 09 package.[33] In the M06-2X-D3 method, the D3 term represents a dispersion correlation and is appropriate for the lignocellulose and IL system.[34−36] Vibrational frequencies were also calculated to verify the stationary structure for all conformations. It is known that the M06-2X-D3/def2SVP level is an excellent compromise between computational cost and accuracy of the computational results.[37] To get more accurate data in the energy, single-point calculations were performed with 3-zeta basis set in the M06-2X/def2TZVP level[38,39] and the diffusion functions (M06-2X/ma-TZVP). Also, the ma-TZVP basis set defined for the atoms referred to in this work was taken from Truhlar's group.[40] The binding energy (ΔE_b) in different computational levels corrected by the basis set superposition error (BSSE) of the complexes is defined as follows:

$$\Delta E_b = E_{complexes} - E_{cellobiose} - E_{cation} - E_{anion} - nE_{H_2O} + \Delta E_{BSSE} \quad (1)$$

where in the BSSE, three fragments were separately defined as cellobiose, anion/cations, and water molecules in the

https://doi.org/10.1021/acsomega.2c04915
ACS Omega 2022, 7, 42170−42180

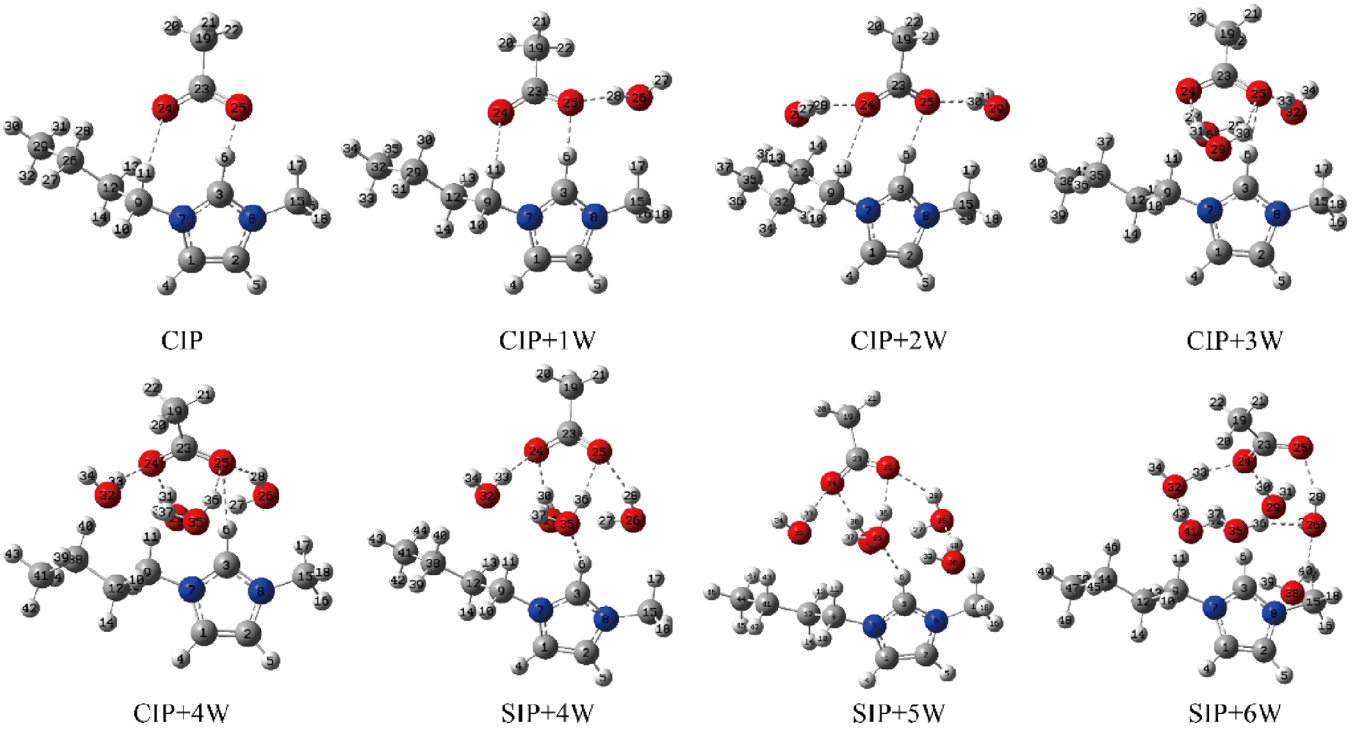

Figure 2. Optimized structures of the contact ion pairs (CIPs) and solvent-separated ion pairs (SIPs) for BmimOAc-nH$_2$O (n = 0−6) clusters.

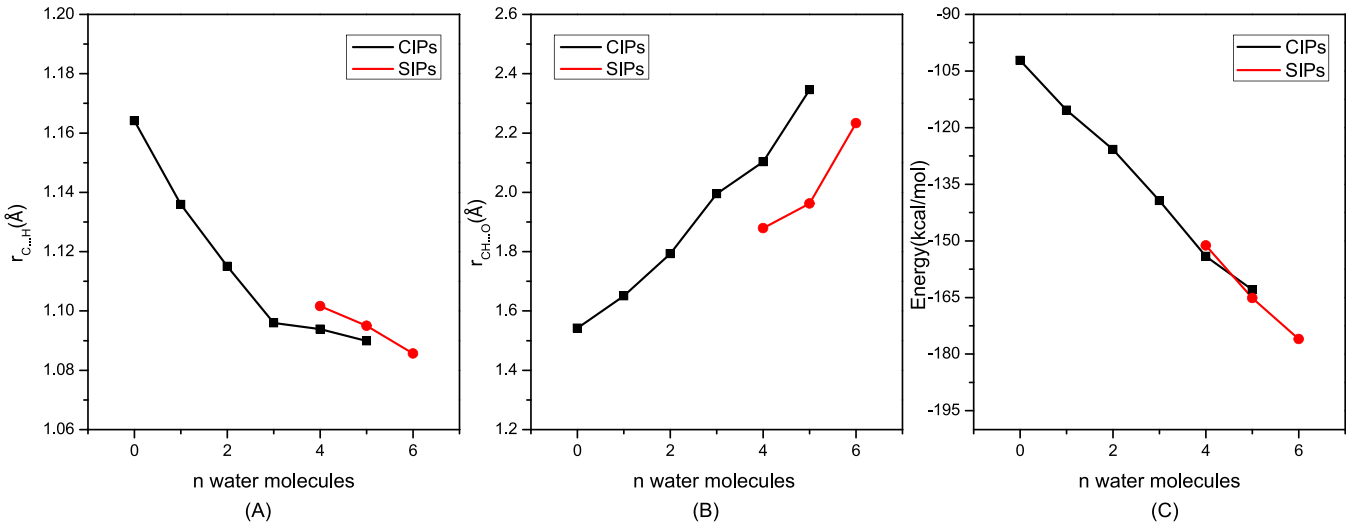

Figure 3. (A) Intramolecular bond $r_{C\cdots H}$ (C3−H6) of Bmim; (B) intermolecular bond $r_{CH\cdots O}$ (C3−H6···O25) and $r_{CH\cdots O}$ (C3−H6 and the nearest oxygen of H$_2$O); (C) total binding energies at the M06-2X/ma-TZVP//M06-2X-D3/def2SVP level for BmimOAc-nH$_2$O (n = 0−6) clusters based on DFT calculations.

cellobiose-ILs-nH$_2$O structures. In addition, the bond characteristics of the cellobiose-ILs-nH$_2$O conformations were further illustrated by the quantum theory of atom in molecules (AIM),[41,42] and the topological properties were performed with the Multiwfn program.[43]

3. RESULTS AND DISCUSSION

As a useful tool to predict the most plausible sites for the electrophilic and nucleophilic attack, quantitative molecular surface analysis of electrostatic potential (ESP)[44,45] of the molecules used in this work is listed in Figure 1. OAc has negative ESP, and Bmim has positive ESP, which are concentrated on the imidazolium rings. Cellulose is modeled by cellobiose due to the limited computational capacity by using DFT calculations. Cellobiose and H$_2$O have dually negative and positive to provide H-bond donors and acceptors. To investigate the cellulose regeneration in ILs and antisolvent mixtures, we studied the microscopic interaction of BmimOAc-nH$_2$O and cellobiose-ILs-nH$_2$O ($0 \le n \le 6$) clusters. Also, we will discuss the geometrics, interaction energies, and the analysis of H-bonds infra.

3.1. Interactions between ILs and nH$_2$O ($0 \le n \le 6$).

The water can be absorbed by most of the ILs in the atmosphere.[46] It is a hot topic to investigate the ILs and H$_2$O system not only in the cellulose regeneration but also in the basic properties of ILs.[47,48] To investigate the interactions

https://doi.org/10.1021/acsomega.2c04915
ACS Omega 2022, 7, 42170−42180

Table 1. Comparison of BSSE (a.u.) and Binding Energies ΔE_b (kcal/mol) of BmimOAc- nH_2O (n = 1−6) at the M06-2X-D3/def2SVP, M06-2X/def2TZVP//M06-2X-D3/def2SVP, and M06-2X/ma-TZVP//M06-2X-D3/def2SVP Levels

	M06-2X-D3/def2SVP		M06-2X/def2TZVP//M06-2X-D3/def2SVP		M06-2X/ma-TZVP//M06-2X-D3/def2SVP	
structure	BSSE	ΔE_b	BSSE	ΔE_b	BSSE	ΔE_b
CIP	0.0163	−105.18	0.0028	−102.95	0.0005	−102.15
CIP + 1W	0.0099	−127.29	0.0046	−115.95	0.0016	−115.36
CIP + 2W	0.0183	−136.85	0.0058	−126.25	0.0022	−125.76
CIP + 3W	0.0340	−149.58	0.0093	−140.22	0.0045	−139.33
CIP + 4W	0.0410	−166.48	0.0106	−155.26	0.0054	−154.11
SIP + 4W	0.0379	−165.94	0.0087	−153.78	0.0063	−151.22
CIP + 5W	0.0474	−178.50	0.0121	−164.48	0.0065	−162.94
SIP + 5W	0.0415	−184.25	0.0091	−167.95	0.0060	−165.16
SIP + 6W	0.0469	−197.39	0.0110	−178.74	0.0070	−176.01

between ILs and antisolvents, we calculated the microstructures of BmimOAc-nH_2O (n = 0−6) through DFT calculations. In the IL-antisolvent structures, there are two kinds of dominant forms, which are contact ion pairs (CIPs) with strong anion−cation interactions and solvent-separated ion pairs (SIPs) with strong ion−solvent interactions.[49,50] A series of BmimOAc-nH_2O (n = 0−6) clusters from different initial guesses were optimized. The structures and energies are listed in Figure S1 and Table S1, respectively. The interaction energy of OAc attacking the C3−H6 and butyl of imidazolium is stronger than the others. Based on this structure, one water molecule was placed around the OAc due to the strong interactions between OAc and H_2O. The water molecules were added one by one based on the structure of the previous one.

To reveal the roles of water molecules in the interactions of anions and cations, the selected CIP and SIP structures of BmimOAc-nH_2O (n = 0−6) clusters are shown in Figure 2. The H-bonds formed between hydroxyls of cellulose and ILs are the driving force for cellulose dissolution, and the competitiveness of H-bonds formed between solvent resistance and ILs is the key to cellulose regeneration.[48,51] Initially, the CIP structures predominated due to the strong electrostatic interaction between Bmim and OAc. With the increasing number of water molecules in the BmimOAc-nH_2O (n = 0−6) clusters, the SIP structures dominate when $n \geq 5$. In addition, the corresponding structural and energy characteristics of the BmimOAc-nH_2O (n = 0−6) clusters are shown in Figures 2 and 3. For the CIP structure, strong H-bonds can be formed between Bmim and OAc with $r_{CH\cdots O}$ (C3−H6···O25) about 1.54 Å. When n = 1, 2, and 3 in the BmimOAc-nH_2O (n = 0−6) clusters, the length of intermolecular bonds (C3−H6···O25) are 1.65, 1.79, and 1.99 Å, respectively. Therefore, it can be found that the H-bonds between anions and cations will be decreased by adding the water molecules. For the intramolecular bond $r_{C\cdots H}$ (C3−H6) of Bmim in the BmimOAc-nH_2O (n = 0−6) clusters, the $r_{C\cdots H}$ of Bmim in the CIP structure is 1.16 Å. When n = 1, 2, and 3, the bond lengths ($r_{C\cdots H}$) of Bmim are 1.14, 1.12, and 1.10 Å, respectively. Hence, the bond length of the imidazole ring (C3−H6) will be decreased with the rising number of H_2O. In the previous study on the 1-ethyl-3-methylimidazolium acetate (EmimOAc) and water clusters,[52] a similarity arises for the inter- and intramolecular bonds with BmimOAc. It further verified that the change of the cation structure provides no new scientific knowledge in relation to the IL/water calculations as the alkyl chain plays no significant role in the hydrogen bonding.

Truhlar *et al.* provided some validations and recommended the ma-TZVP basis set for general-purpose applications of diffusion functions.[40] To compare the influence of diffusion functions on the binding energies, a single-point calculation was carried out with the M06-2X/ma-TZVP level. The BSSE and binding energies of BmimOAc- nH_2O (n = 1−6) with different levels are listed in Table 1. Taking the data of CIP for an example, the binding energies with M06-2X-D3/def2SVP, M06-2X/def2TZVP// M06-2X-D3/def2SVP, and M06-2X/ma-TZVP// M06-2X-D3/def2SVP corrected with BSSE are −105.18, −102.95, and −102.15 kcal/mol. The binding energy with diffusion functions (M06-2X/ma-TZVP) is smaller than that of M06-2X/def2TZVP. The trends of M06-2X/ma-TZVP//M06-2X-D3/def2SVP and M06-2X/def2TZVP//M06-2X-D3/def2SVP are similar. Payal *et al.* reported the structure and dissolution mechanism for cellobiose and xylan in the gas phase and implicit and explicit solvents (water, methanol, and 1,3-dimethylimidazolium acetate).[26] They found that the polarization effect is seen to reduce the energy due to the dielectric constant of the solvent, but the conformers follow the same trend in energy as in the gas phase. Furthermore, the calculated binding energies for all of the conformations in the M06-2X/ma-TZVP//M06-2X-D3/def2SVP level are plotted in Figure 3C. The binding energy of BmimOAc at the M06-2X/ma-TZVP//M06-2X-D3/def2SVP level is −102.15 kcal/mol. When n = 1, 2, and 3 in the BmimOAc-nH_2O (n = 0−6) clusters, the binding energies are −115.36, −125.76, and −139.33 kcal/mol, respectively. Based on the binding energies of the BmimOAc-nH_2O (n = 0−6) clusters, the BmimOAc tended to be a more stable structure with high hydration in an aqueous solution. For the conformations with five or more water molecules, the SIPs are more favorable in BmimOAc/water mixtures. Energy decomposition analysis is a useful tool to investigate the contributions of various energetic components in total interaction energy.[53] To decompose the interaction energies of the complexes, symmetry-adapted perturbation theory (SAPT)[54] was calculated by using Psi4.[55] The interaction energies could be further separated into four components and defined as follows:

$$\Delta E = E_{els} + E_{ex} + E_{ind} + E_{disp}, \text{ kcal/mol} \quad (2)$$

where E_{els}, E_{ex}, E_{ind}, and E_{disp} are the classic electronic interaction, exchange repulsion term, induction term, and dispersion energy, respectively. The energy decomposition analyses of ILs-water for BmimOAc-nH_2O (n = 1−6) structures are presented in Figure 4. Taking the BmimOAc-

https://doi.org/10.1021/acsomega.2c04915
ACS Omega 2022, 7, 42170−42180

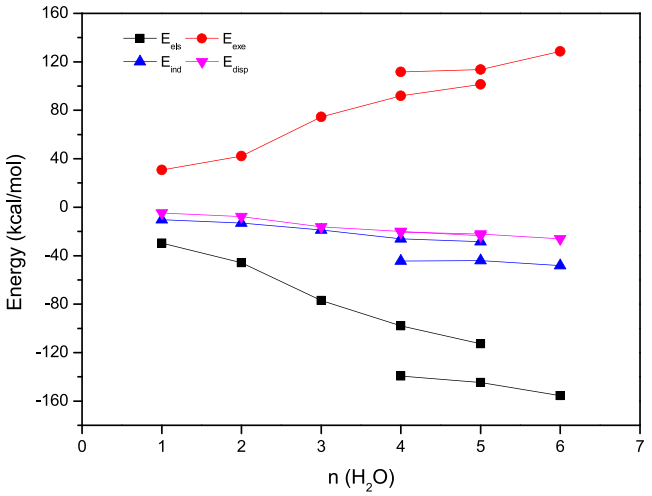

Figure 4. Energy decomposition of interaction energies (in kcal/mol) for BmimOAc-$n$$H_2O$ (n = 1−6).

H_2O for an example, the electronic interaction, exchange repulsion term, induction term, and dispersion energy are −29.65, 30.82, −10.37, and −4.81 kcal/mol, respectively. The electronic interaction and exchange repulsion term occupied about 40% of the total binding energy. For the BmimOAc-$2H_2O$, the electronic interaction, exchange repulsion term, induction term, and dispersion energy are −45.90, 42.19, −12.99, and −7.71 kcal/mol, respectively. With the increasing numbers of water molecules in the BmimOAc-$n$$H_2O$ (n = 1−6), both the induction term and dispersion energy have an increasing tendency. The sum of electronic interaction and exchange repulsion terms as well as the increasing induction and dispersion terms caused the increase of binding energy. In addition, H-bonds can be formed between water molecules and ILs to reduce the interaction of cellulose and ILs. Therefore, cellulose will be regenerated when the water molecules were added to the system.

3.2. Interaction among Cellobiose, Anion/Cation, and $n$$H_2O$ ($0 \le n \le 6$). *3.2.1. Geometrics and Interaction Energy of Cellobiose-Anion/Cation-$n$$H_2O$ ($0 \le n \le 6$).* H-bonds formed between the hydroxyls of cellulose and both anions and cations are the driving force for cellulose dissolution.[56,57] Initially, the structures of cellobiose-OAc and cellobiose-Bmim from different initial guesses (Figures S2 and S3) are optimized at the M06-2X-D3/def2SVP level, and the interaction energies are listed in Tables S2 and S3. The most stable conformations are identified by frequency analysis. It can be found that the interaction energies of cellobiose-OAc appear to be much stronger when the H-bonds are formed between the O of OAc and O2H2, O3H3 sites of cellobiose ,which is consistent with the results reported in the theoretical study of cellulose dissolution.[58,59] Also, the aromatic protons in the imidazolium cation, especially the most acidic H2, prefer to associate with the O of hydroxyls with less steric hindrance.[32]

To investigate the role of antisolvents, we studied the cellobiose-ILs complexes with the increasing quantity of H_2O based on the strongest interaction structures of cellobiose-OAc (Figure 5A) and cellobiose-Bmim (Figure 6A). For the cellobiose-OAc, H-bonds can be formed between the oxygen of OAc and the hydroxyl of cellobiose. The lengths of O52···H15−O14 and O51···H13−O12 bonds are 1.49 and 1.61 Å, respectively. With the increasing number of water molecules in the cellobiose-OAc-$n$$H_2O$ (n = 0−6) clusters, the lengths of O52···H15−O14 and O51···H13−O12 bonds are collected in Figure 7A. It can be found that the interaction between OAc and cellobiose can be weakened with the addition of water molecules. When n = 4 in the cellobiose-OAc-$n$$H_2O$ clusters, the bond lengths of O52···H15−O14 and O51···H13−O12 are 1.60 and 3.39 Å, respectively. The water molecule was inserted into the O51···H13−O12 bond to separate OAc and cellulose. For the structure of cellobiose-Bmim, H-bonds can be formed

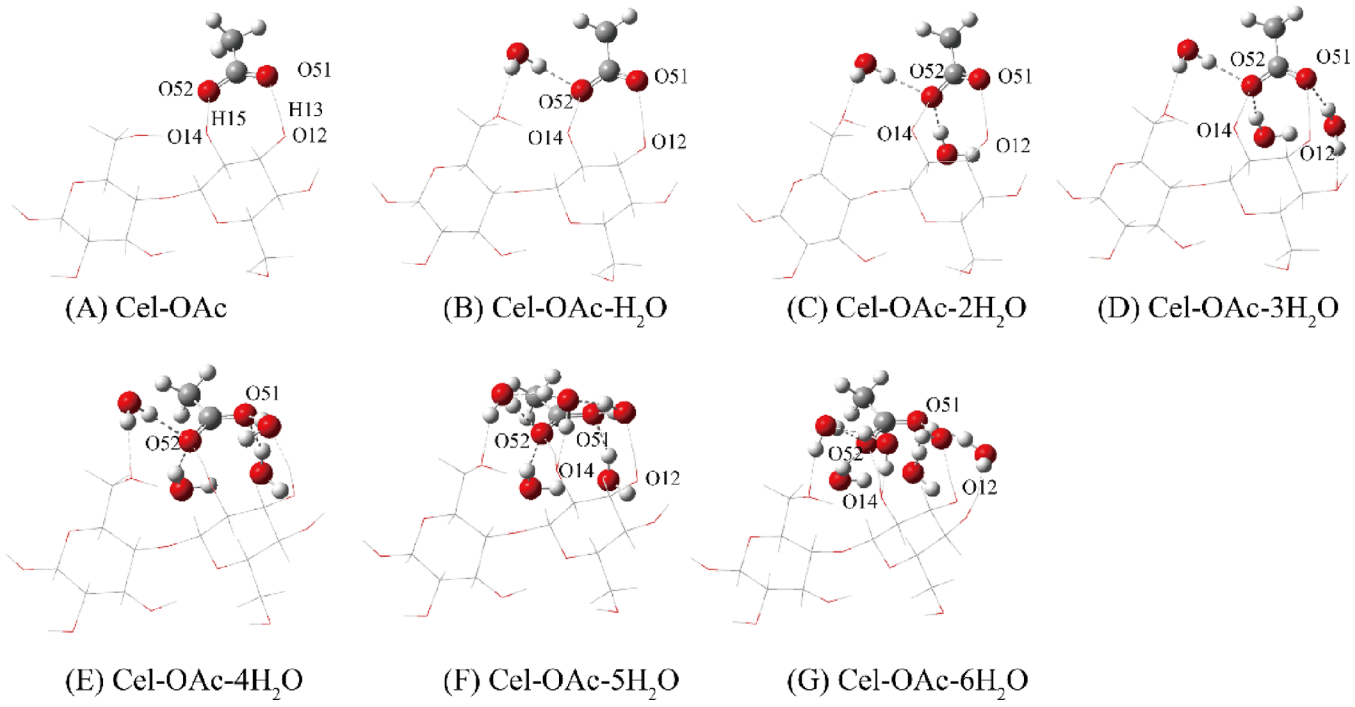

Figure 5. Optimized structures (A−G) for cellobiose-OAc-$n$$H_2O$ (n = 0−6) complexes at the M06-2X-D3/def2SVP level.

https://doi.org/10.1021/acsomega.2c04915
ACS Omega 2022, 7, 42170−42180

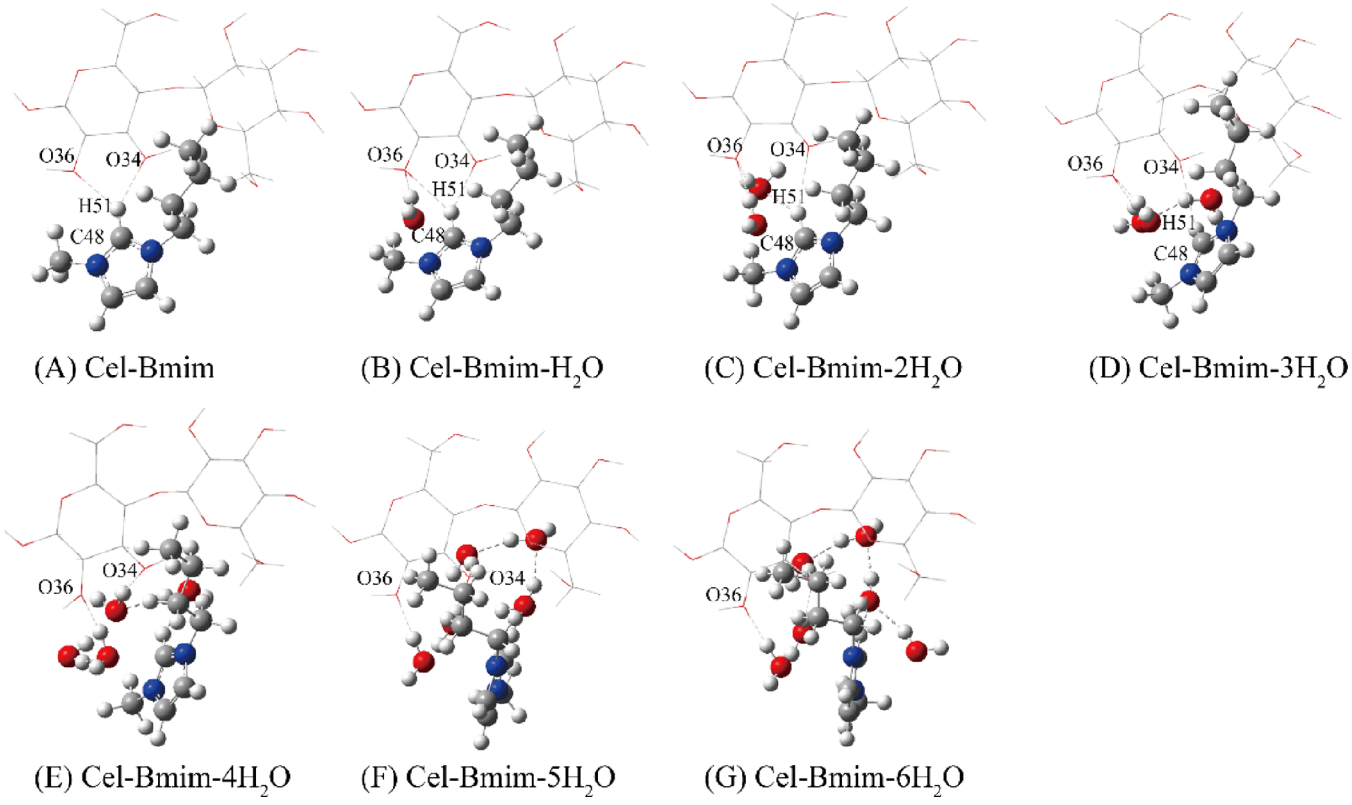

Figure 6. Optimized structures (A−G) for cellobiose-Bmim-nH$_2$O (n = 0−6) complexes at the M06-2X-D3/def2SVP level.

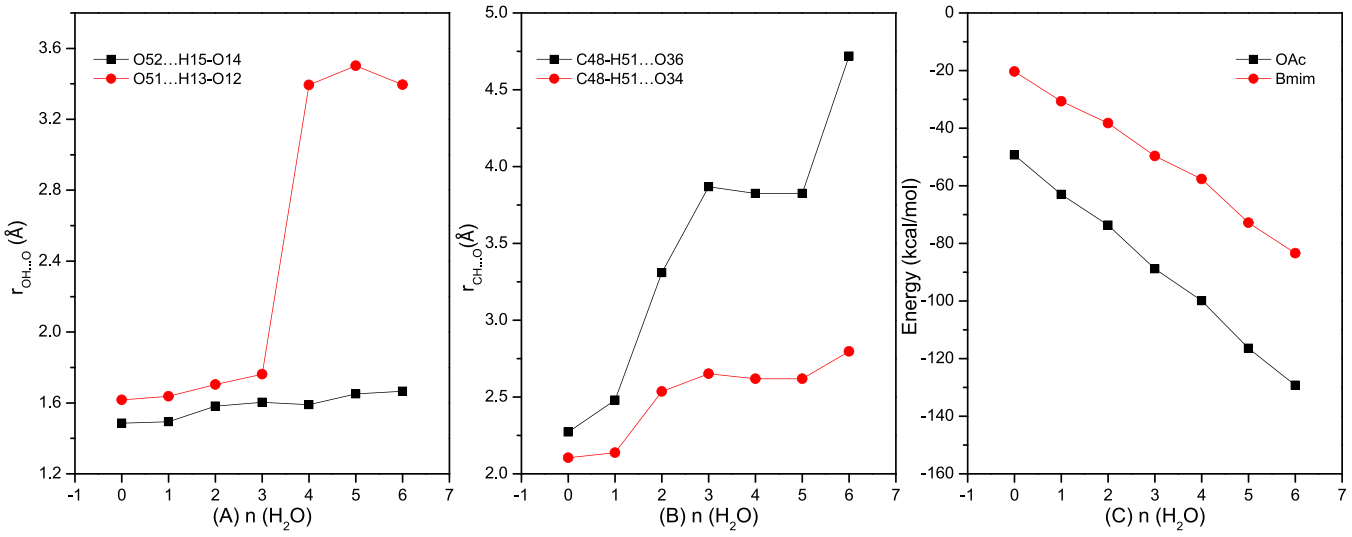

Figure 7. (A) Bond length of H-bonds formed between cellobiose and OAc in cellobiose-OAc-nH$_2$O; (B) bond length of H-bonds formed between cellobiose and Bmim in cellobiose-Bmim-nH$_2$O; (C) total binding energies at the M06-2X/ma-TZVP//M06-2X-D3/def2SVP level for cellobiose-OAc/Bmim-nH$_2$O complexes based on DFT calculations (n = 0−6).

between the C2−H of Bmim and the oxygen of cellobiose. The lengths of O36···H51−C48 and O34···H51−C48 are 2.10 and 2.27 Å, respectively. With the increasing number of water molecules in the cellobiose-Bmim-nH$_2$O (n = 0−6) clusters, the lengths of O36···H51−C48 and O34···H51−C48 bonds as well as the structures are summarized in Figure 7B and Figure 6, respectively. It could be found that the length of H-bonds formed between Bmim and cellobiose will be increased with the addition of water molecules. Taking the cellobiose-Bmim-3H$_2$O structure as an example, the lengths of O36···H51−C48 and O34···H51−C48 are 3.83 and 2.62 Å, respectively. Therefore, the H-bonds formed among cellobiose, anions, and cations will be weakened after the addition of water molecules, resulting in a decrease in cellulose dissolution and achieving cellulose regeneration. In addition, the binding energies corrected by BSSE of cellobiose-Bmim-nH$_2$O and cellobiose-OAc-nH$_2$O (n = 0−6) clusters with the M06-2X/ma-TZVP//M06-2X-D3/def2SVP level are shown in Figure 7C. When n = 0, the binding energies of cellobiose-Bmim and cellobiose-OAc are −20.36 and −49.37, kcal/mol. The

https://doi.org/10.1021/acsomega.2c04915
ACS Omega 2022, 7, 42170−42180

interaction energies of cellobiose-OAc-$n$$H_2O$ are stronger than that of cellobiose-Bmim-$n$$H_2O$ with the same water molecule. With the increasing numbers of water in cellobiose-OAc-$n$$H_2O$ (n = 0−6) clusters, the binding energies are −49.37, −63.04, −73.63, −88.83, −99.89, −116.38 and −129.24 kcal/mol, respectively. The cellobiose-ILs tend to be a more stable structure with high hydration in an aqueous solution.

3.2.2. AIM Analysis of Cellobiose-Anion/Cation-nH_2O (0 ≤ n ≤ 6). To discuss the bonding properties of the intermolecular interactions of the cellobiose- anion/cation-$n$$H_2O$ clusters, atom in molecules theory (AIM) analysis was employed to reveal the chemical bonds of the interaction in this part. AIM analysis is a universally applicable tool that can clarify many types of interactions by the topological properties at the bond critical points (BCP).[60−62] Lipkowski *et al.* proposed two topology criteria, which were the electron density (ρ_{BCP}) and Laplacian of electron density ($\nabla^2\rho_{BCP}$) for the existence of H-bonds in the closed shell when the ρ_{BCP} is in 0.002−0.034 a.u. and $\nabla^2\rho_{BCP}$ is in 0.024−0.139 a.u..[63] Different kinds of H-bonds were considered to be formed in terms of $\nabla^2\rho_{BCP}$ and H_{BCP} (weak H-bonds, $\nabla^2\rho_{BCP} > 0$, $H_{BCP} > 0$; medium H-bonds, $\nabla^2\rho_{BCP} > 0$, $H_{BCP} < 0$; and strong H-bonds, $\nabla^2\rho_{BCP} < 0$, $H_{BCP} < 0$).[64] Half of the potential energy density ($V(r)$) was the energy of H-bonds [X−H···O (X = C, N, O)].[65] Based on the results of the AIM analysis, the value of ρ_{BCP}, $\nabla^2\rho_{BCP}$, and H_{BCP} of the H-bonds in Cel-OAc-$n$$H_2O$ and Cel-Bmim-$n$$H_2O$ clusters calculated at the M06-2X-D3/def2SVP level are summarized in Table 2. In the conformation of Cel-OAc, the ρ_{BCP} of O52···H15−O14 and O51···H13−O12 are 0.079 and 0.055 a.u., respectively. When the water molecule was added to the system, taking the Cel-OAc-H_2O for an example, the H-bonds (O52···H15−O14 and O51···H13−O12) formed between OAc and the hydroxyl of cellulose will be decreased. Furthermore, H-bonds can also be formed between the H_2O and OAc due to the ρ_{BCP} of the O52···H55−O53 bond being 0.032 a.u.. Therefore, the interactions between cellulose and OAc will be weakened with the addition of water molecules. For the Cel-Bmim-$n$$H_2O$ clusters, H-bonds and van der Waals force interactions are the main interaction patterns between cellulose and cations. Taking the Cel-Bmim structure as an example, the energies of C48−H51···O36 and C48−H51···O34 H-bonds (half of the $V(r)$) are −0.0055 and −0.0073 a.u.. When the water molecules were introduced into the cellulose−cation system, H-bonds will be formed between the hydroxyl of cellulose and H_2O. In the Cel-Bmim-H_2O structure, the energy of the H-bond (O71−H73···O36) formed between H_2O and the hydroxyl (cellulose) is −0.0104 a.u.. The H-bonds formed between cellulose and Bmim will be decreased because the energy of C48−H51···O36 and C48−H51···O34 are −0.0036 and −0.0068 a.u.. So, the water molecule will hinder the interaction of cellulose and ILs by forming H-bonds with the hydroxyl of cellulose and ILs to make the cellulose regeneration.

3.2.3. IGMH Analysis of Cellobiose-Anion/Cation-nH_2O (0 ≤ n ≤ 6). As a practical tool for investigating noncovalent interactions, independent gradient model (IGM) analysis has been popular in the visual analysis of intramolecular and intermolecular interactions.[66,67] However, there are some shortcomings of the IGM map such as the bulgy isosurfaces and poor graphical effect. As a new method for visualizing the interactions in chemical systems, the independent gradient model based on Hirshfeld partition (IGMH) replaced the free-state atomic densities involved in the IGM with atomic densities derived by Hirshfeld partition.[68] IGMH has a better graphical effect than IGM and overcomes known problems in IGM. The intermolecular interaction isosurface based on IGM and IGMH is plotted in Figure S4 and Figure 8. Taking the structure of Cel-OAc as an example (Figure 8A), two blue isosurface areas around the oxygen of OAc and hydroxyl of cellulose indicate that strong H-bonds can be formed between the cellobiose and anions. There is also a π-stacking around the ring of the glucose unit with OAc. Furthermore, the isosurface area of IGMH with the same isovalue is smaller than that of IGM. IGMH has a better capacity than IGM in revealing chemical bond interactions since actual electron density is involved in the definition of IGMH. In the cellobiose-OAc-H_2O structure (Figure 8B), another two isosurface areas around H_2O can be found. It shows that H-bonds can be formed among H_2O, hydroxyl (cellulose), and oxygen (OAc). For the IGMH analysis of the cellobiose-Bmim structure (Figure 8D), H-bonds can be formed between the C2−H of imidazole and hydroxyl of cellulose, and there is also a large area for the van der Waals interaction around the alkyl chain of Bmim and cellulose. With the addition of water molecules, the water molecules tend to form H-bonds with the hydroxyl of cellobiose to separate the interactions of cellobiose and Bmim. It can be concluded that the water molecules can form H-bonds with the hydroxyl of cellobiose and OAc to reduce the

Table 2. Electron Density (ρ_{BCP}), Laplacian of the Electron Density ($\nabla^2\rho_{BCP}$), Energy Density (H_{BCP}), and Potential Energy Density ($V(r)$) of Cel-OAc-$n$$H_2O$ and Cel-Bmim-$n$$H_2O$ ($0 \le n \le 2$) (a.u.)

structure	H-Bond	ρ_{BCP}	$\nabla^2\rho_{BCP}$	H_{BCP} (10^{-3} a.u.)	$V(r)$
Cel-OAc	O52···H15−O14	0.079	0.145	−26.685	−0.090
	O51···H13−O12	0.055	0.164	−5.500	−0.052
Cel-OAc-H_2O	O52···H15−O14	0.077	0.157	−23.861	−0.087
	O51···H13−O12	0.052	0.160	−3.656	−0.047
	O52···H55−O53	0.032	0.115	1.870	−0.025
Cel-OAc-2H_2O	O52···H15−O14	0.061	0.170	−9.023	−0.061
	O51···H13−O12	0.043	0.149	0.505	−0.036
	O52···H55−O53	0.030	0.107	1.704	−0.023
	O43···H54−O53	0.023	0.075	0.122	−0.018
Cel-Bmim	C48−H51···O36	0.014	0.050	0.752	−0.011
	C48−H51···O34	0.019	0.063	0.670	−0.015
Cel-Bmim-H_2O	C48−H51···O36	0.010	0.036	0.871	−0.007
	C48−H51···O34	0.018	0.059	0.508	−0.014
	O71−H73···O36	0.027	0.105	2.701	−0.021
Cel-Bmim-2H_2O	C48−H51···O34	0.009	0.028	0.495	−0.006
	O71−H73···O36	0.026	0.102	3.016	−0.019
	O74−H76···O36	0.028	0.099	1.683	−0.021

https://doi.org/10.1021/acsomega.2c04915
ACS Omega 2022, 7, 42170−42180

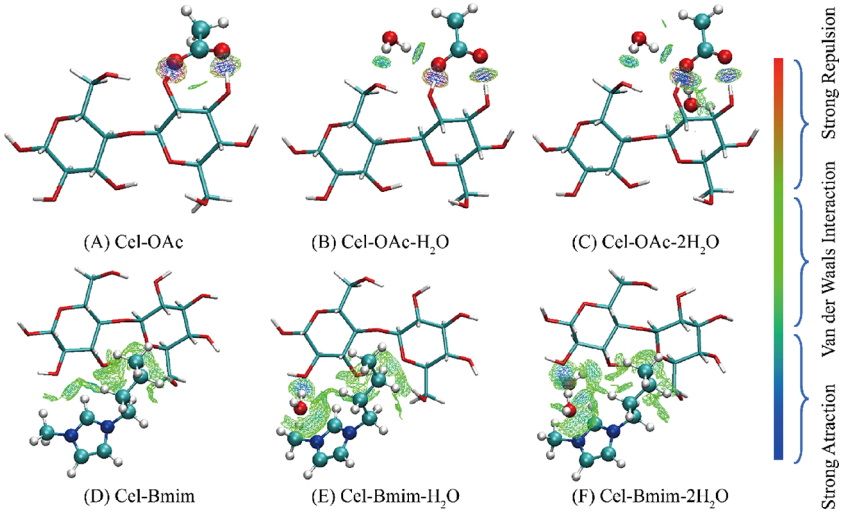

Figure 8. Intermolecular interaction isosurface of (A−C) cellobiose-OAc-nH$_2$O (n = 0−2) (isovalue = 0.01 a.u.) and (D−F) cellobiose-OAc/Bmim-nH$_2$O (n = 0−2) (isovalue = 0.005 a.u.). Blue indicates strong attractive interaction, green indicates the van der Waals interaction, and red indicates the steric effect.

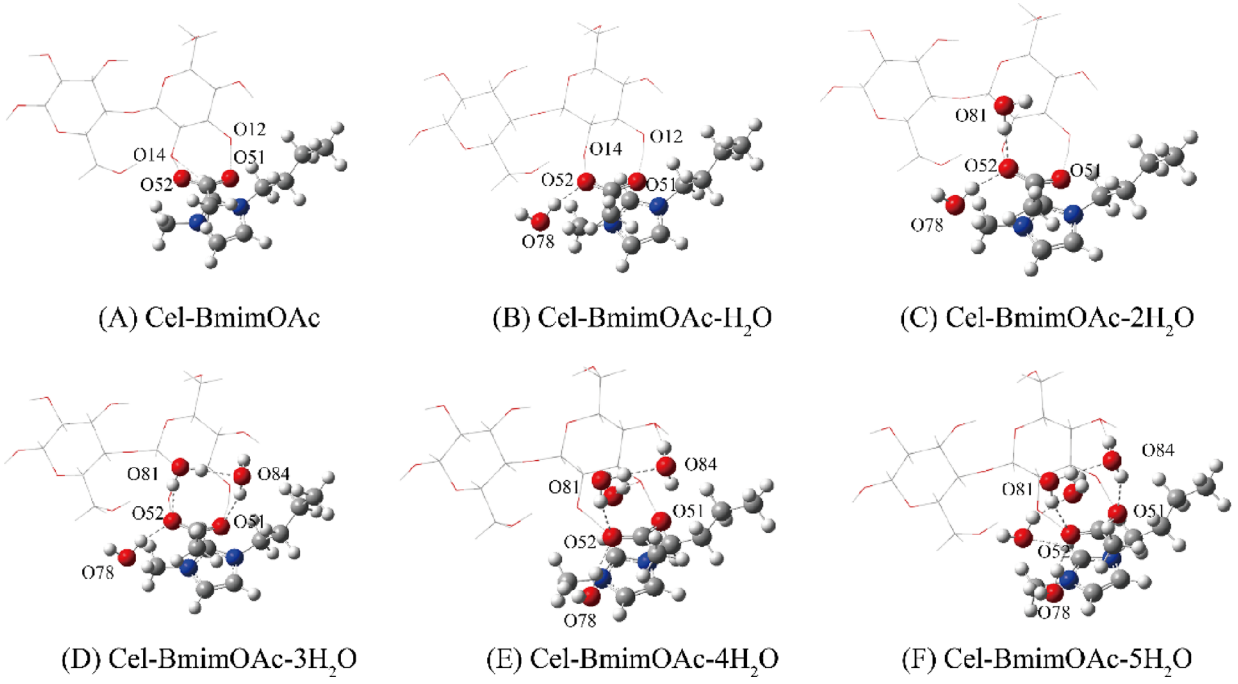

Figure 9. Optimized structures (A−F) of Cellobiose-BmimOAc-nH$_2$O (n = 0−5) complexes at the M06-2X-D3/def2SVP level.

interactions of cellulose-ILs. Therefore, the cellulose will be regenerated when the waters were brought into the system.

3.3. Interaction among Cellobiose, ILs, and nH$_2$O (0 ≤ n ≤ 6). Single ions are the threshold to understand the cellulose regeneration in ILs and antisolvent mixtures. Also, the anions and cations may appear in the form of ion pairs due to the strong electrostatic interactions in the real IL system.[69] To investigate the regeneration of cellulose in the ILs/H$_2$O mixture, we optimized a series of cellobiose-BmimOAc-nH$_2$O (n = 0−6) clusters at the M06-2X-D3/def2SVP level. Similar to the structures of cellobiose-anions/cations-nH$_2$O, some selected structures of cellobiose-ion pairs-nH$_2$O are shown in Figure 9. In addition, the length of H-bonds formed between anion/cation and cellobiose as well as the binding energy of cellobiose-BmimOAc-nH$_2$O (n = 0−6) with the increasing number of water molecules are shown in Figure 10. Initially, H-bonds formed between the hydroxyls of cellobiose and the oxygens of OAc (O52···H15−O14 and O51···H13−O12) are 1.51045 and 1.55869 Å, respectively. With the increasing number of water molecules in the cellobiose-BmimOAc-nH$_2$O clusters, the bond lengths of H-bonds formed between cellobiose and OAc tend to increase. Because of the slant of OAc, the bond length of H-bonds formed between cellobiose and one of the oxygen of OAc was shortened. The lengths of H-bonds formed between cellobiose and Bmim were elongated by the water molecules inserted in the system. Therefore, the interactions between cellobiose and ILs were weakened with the increase of water molecules and it will be beneficial for cellulose regeneration. In addition, the binding energies corrected by BSSE of cellobiose-BmimOAc-nH$_2$O (n = 0−6)

https://doi.org/10.1021/acsomega.2c04915
ACS Omega 2022, 7, 42170−42180

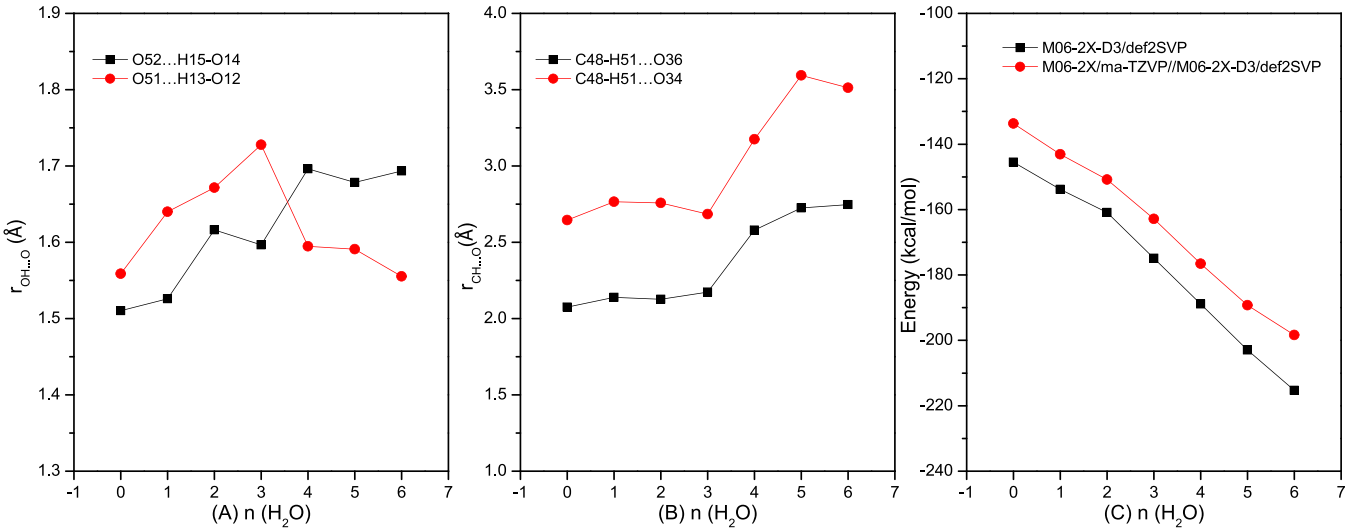

Figure 10. (A) Bond length of H-bonds formed between cellobiose and OAc in cellobiose-BmimOAc-$n$$H_2O$; (B) bond length of H-bonds formed between cellobiose and Bmim in cellobiose-BmimOAc-$n$$H_2O$; (C) total binding energies for cellobiose-BmimOAc-$n$$H_2O$ complexes at different levels (M06-2X-D3/def2SVP and M06-2X/ma-TZVP//M06-2X-D3/def2SVP) corrected by BSSE (n = 0−6).

clusters with M06-2X-D3/def2SVP and M06-2X/ma-TZVP//M06-2X-D3/def2SVP levels are shown in Figure 10C. The binding energy in M06-2X/ma-TZVP//M06-2X-D3/def2SVP was smaller than that of M06-2X-D3/def2SVP. However, the tendency with different levels is similar. With the increasing numbers of water molecules, the binding energies become stronger than the previous one. Furthermore, H-bonds can be formed among H_2O, the hydroxyl of cellulose, and the oxygen of OAc based on the optimized structures of cellobiose-BmimOAc-$n$$H_2O$ (n = 0−6) clusters. The water molecules were introduced into the system and hindered the interaction of cellulose and ILs to make the cellulose regeneration.

4. CONCLUSIONS

In this work, the cellulose regeneration mechanism in a BmimOAc/water mixture was studied by density functional theory (DFT) calculations. It could be found that contact ion pairs (CIPs) are the main structures in the BmimOAc-$n$$H_2O$ ($0 \leq n \leq 4$) clusters. When $n \geq 5$ in the BmimOAc-$n$$H_2O$ clusters, the solvent-separated ion pairs (SIPs) play a dominant position in the system. With the increasing numbers of water molecules, the cation−anion interaction can be separated by water to reduce the effects of ILs on cellulose dissolution. Furthermore, the BmimOAc-$n$$H_2O$ and cellobiose-IL (n = 0−6) complexes tend to be a more stable structure with high hydration in an aqueous solution. When the antisolvent is added to the system, H-bonds can be formed among H_2O, the hydroxyl of cellulose, and the oxygen of OAc. Therefore, the interactions between cellobiose and ILs will be decreased to promote cellulose regeneration. Overall, insightful structural properties for the cellulose regeneration in BmimOAc/H_2O mixtures at a microscopic level are provided in this work. It would provide some basic aid to understand the mechanism of cellulose regeneration in antisolvents.

■ ASSOCIATED CONTENT

Supporting Information

The Supporting Information is available free of charge at https://pubs.acs.org/doi/10.1021/acsomega.2c04915.

Structures, H-bonds, and interaction energies between cellulose and OAc/Bmim; optimized coordinates of DFT-calculated BmimOAc-$n$$H_2O$, cellobiose-Bmim-$n$$H_2O$, and cellobiose-Bmim-$n$$H_2O$, and cellobiose-BmimOAc-$n$$H_2O$ (n = 0−6) clusters (PDF)

■ AUTHOR INFORMATION

Corresponding Authors

Zhaoyang Ju − *College of Chemical & Material Engineering, Quzhou University, Quzhou 324000, China*; orcid.org/0000-0001-7989-5414; Email: jzy@qzc.edu.cn

Chengsheng Ge − *College of Chemical & Material Engineering, Quzhou University, Quzhou 324000, China*; Email: gechengsheng@qzc.edu.cn

Authors

Lanlan Fu − *College of Chemical & Material Engineering, Quzhou University, Quzhou 324000, China*

Mengting Yu − *College of Chemical & Material Engineering, Quzhou University, Quzhou 324000, China*

Huaying Luo − *Xianhe Co., Ltd., Quzhou 324022, China*

Cheng Zhang − *Xianhe Co., Ltd., Quzhou 324022, China*

Ximing Zhang − *College of Biosystems Engineering and Food Science, Zhejiang University, Hangzhou 310058, China*; orcid.org/0000-0002-4889-8791

Haixiang Cheng − *College of Chemical & Material Engineering, Quzhou University, Quzhou 324000, China*

Minjia Zheng − *College of Chemical & Material Engineering, Quzhou University, Quzhou 324000, China*

Lu Jin − *College of Chemical & Material Engineering, Quzhou University, Quzhou 324000, China*

Complete contact information is available at: https://pubs.acs.org/10.1021/acsomega.2c04915

Notes

The authors declare no competing financial interest.

■ ACKNOWLEDGMENTS

This research was funded by the Key R&D Program of Zhejiang Province (no. 2021C02031), the Science and

Technology Project of Quzhou City (nos. 2021Z01 and 2020K09), the National College Student Innovation and Entrepreneurship Training Program (no. 202111488046), the Science and Technology Project of Qujiang District, Quzhou City (nos. QJ2019J001, QJ2020012, QJ2020022, QJ2021038), and Lab Open Project (no. KFXM202204). The work was carried out at Shanxi Supercomputing Center of China, and the calculations were performed on TianHe-2.

REFERENCES

(1) Klemm, D.; Heublein, B.; Fink, H. P.; Bohn, A. Cellulose: Fascinating Biopolymer and Sustainable Raw Material. *Angew. Chem., Int. Ed.* **2005**, *44*, 3358−3393.
(2) Nongbe, M. C.; Bretel, G.; Ekou, T.; Ekou, L.; Yao, B. K.; Le Grognec, E.; Felpin, F.-X. Cellulose paper grafted with polyamines as powerful adsorbent for heavy metals. *Cellulose* **2018**, *25*, 4043−4055.
(3) Emam, H. E. Generic strategies for functionalization of cellulosic textiles with metal salts. *Cellulose* **2019**, *26*, 1431−1447.
(4) Satari, B.; Karimi, K.; Kumar, R. Cellulose solvent-based pretreatment for enhanced second-generation biofuel production: a review. *Sustainable Energy Fuels* **2019**, *3*, 11−62.
(5) Sharma, H. K.; Xu, C.; Qin, W. Biological Pretreatment of Lignocellulosic Biomass for Biofuels and Bioproducts: An Overview. *Waste Biomass Valoriz.* **2019**, *10*, 235−251.
(6) O'Sullivan, A. C. Cellulose: the structure slowly unravels. *Cellulose* **1997**, *4*, 173−207.
(7) Samayam, I. P.; Hanson, B. L.; Langan, P.; Schall, C. A. Ionic-Liquid Induced Changes in Cellulose Structure Associated with Enhanced Biomass Hydrolysis. *Biomacromolecules* **2011**, *12*, 3091−3098.
(8) Notley, S. M.; Pettersson, B.; Wågberg, L. Direct Measurement of Attractive van der Waals' Forces between Regenerated Cellulose Surfaces in an Aqueous Environment. *J. Am. Chem. Soc.* **2004**, *126*, 13930−13931.
(9) Demain, A. L.; Newcomb, M.; Wu, J. H. D. Cellulase, Clostridia, and Ethanol. *Microbiol. Mol. Biol. Rev.* **2005**, *69*, 124−154.
(10) Zhu, S.; Wu, Y.; Chen, Q.; Yu, Z.; Wang, C.; Jin, S.; Ding, Y.; Wu, G. Dissolution of cellulose with ionic liquids and its application: a mini-review. *Green Chem.* **2006**, *8*, 325−327.
(11) Lei, Z.; Chen, B.; Koo, Y. M.; Macfarlane, D. R. Introduction: Ionic Liquids. *Chem. Rev.* **2017**, *117*, 6633−6635.
(12) Zakrzewska, M. E.; Bogel-Łukasik, E.; Bogel-Łukasik, R. Solubility of Carbohydrates in Ionic Liquids. *Energy Fuels* **2010**, *24*, 737−745.
(13) Freudenmann, D.; Wolf, S.; Wolff, M.; Feldmann, C. Ionic Liquids: New Perspectives for Inorganic Synthesis? *Angew. Chem., Int. Ed.* **2011**, *50*, 11050−11060.
(14) Swatloski, R. P.; Spear, S. K.; Holbrey, J. D.; Rogers, R. D. Dissolution of Cellose with Ionic Liquids. *J. Am. Chem. Soc.* **2002**, *124*, 4974−4975.
(15) Uto, T.; Yamamoto, K.; Kadokawa, J.-i. Cellulose Crystal Dissolution in Imidazolium-Based Ionic Liquids: A Theoretical Study. *J. Phys. Chem. B* **2018**, *122*, 258−266.
(16) Wang, H.; Gurau, G.; Rogers, R. D. Ionic liquid processing of cellulose. *Chem. Soc. Rev.* **2012**, *41*, 1519−1537.
(17) Badgujar, K. C.; Bhanage, B. M. Factors governing dissolution process of lignocellulosic biomass in ionic liquid: Current status, overview and challenges. *Bioresour. Technol.* **2015**, *178*, 2−18.
(18) Zhang, J.; Wu, J.; Yu, J.; Zhang, X.; He, J.; Zhang, J. Application of ionic liquids for dissolving cellulose and fabricating cellulose-based materials: state of the art and future trends. *Mater. Chem. Front.* **2017**, *1*, 1273−1290.
(19) Medronho, B.; Lindman, B. Brief overview on cellulose dissolution/regeneration interactions and mechanisms. *Adv. Colloid Interface Sci.* **2015**, *222*, 502−508.
(20) Li, J.; Lu, S.; Liu, F.; Qiao, Q.; Na, H.; Zhu, J. Structure and Properties of Regenerated Cellulose Fibers Based on Dissolution of Cellulose in a CO_2 Switchable Solvent. *ACS Sustainable Chem. Eng.* **2021**, *9*, 4744−4754.
(21) Zhu, Q.; Zhou, X.; Ma, J.; Liu, X. Preparation and Characterization of Novel Regenerated Cellulose Films via Sol−Gel Technology. *Ind. Eng. Chem. Res.* **2013**, *52*, 17900−17906.
(22) Hauru, L. K. J.; Hummel, M.; King, A. W. T.; Kilpeläinen, I.; Sixta, H. Role of Solvent Parameters in the Regeneration of Cellulose from Ionic Liquid Solutions. *Biomacromolecules* **2012**, *13*, 2896−2905.
(23) Ju, Z.; Xiao, W.; Yao, X.; Tan, X.; Simmons, B. A.; Sale, K. L.; Sun, N. Theoretical study on the microscopic mechanism of lignin solubilization in Keggin-type polyoxometalate ionic liquids. *Phys. Chem. Chem. Phys.* **2020**, *22*, 2878−2886.
(24) Zhang, Y.; He, H.; Liu, Y.; Wang, Y.; Huo, F.; Fan, M.; Adidharma, H.; Li, X.; Zhang, S. Recent progress in theoretical and computational studies on the utilization of lignocellulosic materials. *Green Chem.* **2019**, *21*, 9−35.
(25) Gupta, K. M.; Jiang, J. Cellulose dissolution and regeneration in ionic liquids: A computational perspective. *Chem. Eng. Sci.* **2015**, *121*, 180−189.
(26) Payal, R. S.; Bharath, R.; Periyasamy, G.; Balasubramanian, S. Density Functional Theory Investigations on the Structure and Dissolution Mechanisms for Cellobiose and Xylan in an Ionic Liquid: Gas Phase and Cluster Calculations. *J. Phys. Chem. B* **2012**, *116*, 833−840.
(27) Zhao, Y.; Liu, X.; Wang, J.; Zhang, S. Insight into the Cosolvent Effect of Cellulose Dissolution in Imidazolium-Based Ionic Liquid Systems. *J. Phys. Chem. B* **2013**, *117*, 9042−9049.
(28) Liu, H.; Sale, K. L.; Simmons, B. A.; Singh, S. Molecular Dynamics Study of Polysaccharides in Binary Solvent Mixtures of an Ionic Liquid and Water. *J. Phys. Chem. B* **2011**, *115*, 10251−10258.
(29) Xu, A.; Guo, X.; Xu, R. Understanding the dissolution of cellulose in 1-butyl-3-methylimidazolium acetate+DMAc solvent. *Int. J. Biol. Macromol.* **2015**, *81*, 1000−1004.
(30) Andanson, J.-M.; Bordes, E.; Devémy, J.; Leroux, F.; Pádua, A. A. H.; Gomes, M. F. C. Understanding the role of co-solvents in the dissolution of cellulose in ionic liquids. *Green Chem.* **2014**, *16*, 2528−2538.
(31) Yao, Y.; Li, Y.; Liu, X.; Zhang, X.; Wang, J.; Yao, X.; Zhang, S. Mechanistic study on the cellulose dissolution in ionic liquids by density functional theory. *Chin. J. Chem. Eng.* **2015**, *23*, 1894−1906.
(32) Cao, B.; Du, J.; Du, D.; Sun, H.; Zhu, X.; Fu, H. Cellobiose as a model system to reveal cellulose dissolution mechanism in acetate-based ionic liquids: Density functional theory study substantiated by NMR spectra. *Carbohydr. Polym.* **2016**, *149*, 348−356.
(33) Frisch, M. J.; Trucks, G. W.; Schlegel, H. B.; Scuseria, G. E.; Robb, M. A.; Cheeseman, J. R.; Scalmani, G.; Barone, V.; Petersson, G. A.; Nakatsuji, H.; Li, X.; Caricato, M.; Marenich, A. V.; Bloino, J.; Janesko, B. G.; Gomperts, R.; Mennucci, B.; Hratchian, H. P.; Ortiz, J. V.; Izmaylov, A. F.; Sonnenberg, J. L.; Williams; Ding, F.; Lipparini, F.; Egidi, F.; Goings, J.; Peng, B.; Petrone, A.; Henderson, T.; Ranasinghe, D.; Zakrzewski, V. G.; Gao, J.; Rega, N.; Zheng, G.; Liang, W.; Hada, M.; Ehara, M.; Toyota, K.; Fukuda, R.; Hasegawa, J.; Ishida, M.; Nakajima, T.; Honda, Y.; Kitao, O.; Nakai, H.; Vreven, T.; Throssell, K.; Montgomery, Jr., J. A.; Peralta, J. E.; Ogliaro, F.; Bearpark, M. J.; Heyd, J. J.; Brothers, E. N.; Kudin, K. N.; Staroverov, V. N.; Keith, T. A.; Kobayashi, R.; Normand, J.; Raghavachari, K.; Rendell, A. P.; Burant, J. C.; Iyengar, S. S.; Tomasi, J.; Cossi, M.; Millam, J. M.; Klene, M.; Adamo, C.; Cammi, R.; Ochterski, J. W.; Martin, R. L.; Morokuma, K.; Farkas, O.; Foresman, J. B.; Fox, D. J. *Gaussian 09*, Wallingford, CT, 2013.
(34) Janesko, B. G. Modeling interactions between lignocellulose and ionic liquids using DFT-D. *Phys. Chem. Chem. Phys.* **2011**, *13*, 11393−11401.
(35) Grimme, S.; Ehrlich, S.; Goerigk, L. Effect of the damping function in dispersion corrected density functional theory. *J. Comput. Chem.* **2011**, *32*, 1456−1465.
(36) Grimme, S.; Antony, J.; Ehrlich, S.; Krieg, H. A consistent and accurate ab initio parametrization of density functional dispersion

https://doi.org/10.1021/acsomega.2c04915
ACS Omega 2022, 7, 42170−42180

correction (DFT-D) for the 94 elements H-Pu. *J. Chem. Phys.* **2010**, *132*, 154104.
(37) Dáaz-Oviedo, C. D.; Maji, R.; List, B. The Catalytic Asymmetric Intermolecular Prins Reaction. *J. Am. Chem. Soc.* **2021**, *143*, 20598−20604.
(38) Turner, J. A.; Adrianov, T.; Zakaria, M. A.; Taylor, M. S. Effects of Configuration and Substitution on C−H Bond Dissociation Enthalpies in Carbohydrate Derivatives: A Systematic Computational Study. *J. Org. Chem.* **2022**, *87*, 1421−1433.
(39) Ju, Z.; Feng, S.; Ren, L.; Lei, T.; Cheng, H.; Yu, M.; Ge, C. Probing the mechanism of the conversion of methyl levulinate into γ-valerolactone catalyzed by Al(OiPr)3 in an alcohol solvent: a DFT study. *RSC Adv.* **2022**, *12*, 2788−2797.
(40) Zheng, J.; Xu, X.; Truhlar, D. G. Minimally augmented Karlsruhe basis sets. *Theor. Chem. Acc.* **2011**, *128*, 295−305.
(41) Fuster, F.; Grabowski, S. J. Intramolecular hydrogen bonds: the QTAIM and ELF characteristics. *J. Phys. Chem. A* **2011**, *115*, 10078−10086.
(42) Bader, R. F. W.; Matta, C. F. Atoms in molecules as non-overlapping, bounded, space-filling open quantum systems. *Found. Chem.* **2012**, *15*, 253−276.
(43) Lu, T.; Chen, F. Multiwfn: A multifunctional wavefunction analyzer. *J. Comput. Chem.* **2012**, *33*, 580−592.
(44) Fu, R.; Lu, T.; Chen, F.-W. Comparing Methods for Predicting the Reactive Site of Electrophilic Substitution. *Acta Phys.-Chim. Sin.* **2014**, *30*, 628−639.
(45) Wang, Z.; Liu, Y.; Zheng, B.; Zhou, F.; Jiao, Y.; Liu, Y.; Ding, X.; Lu, T. A theoretical investigation on Cu/Ag/Au bonding in XH2P···MY(X = H, CH3, F, CN, NO2; M = Cu, Ag, Au; Y = F, Cl, Br, I) complexes. *J. Chem. Phys.* **2018**, *148*, 194106.
(46) Visser, A. E.; Swatloski, R. P.; Reichert, W. M.; Griffin, S. T.; Rogers, R. D. Traditional Extractants in Nontraditional Solvents: Groups 1 and 2 Extraction by Crown Ethers in Room-Temperature Ionic Liquids. *Ind. Eng. Chem. Res.* **2000**, *39*, 3596−3604.
(47) Guo, S.; Chen, F.; Liu, L.; Li, Y.; Liu, X.; Jiang, K.; Liu, R.; Zhang, S. Effects of the Water Content on the Transport Properties of Ionic Liquids. *Ind. Eng. Chem. Res.* **2019**, *58*, 19661−19669.
(48) Parthasarathi, R.; Balamurugan, K.; Shi, J.; Subramanian, V.; Simmons, B. A.; Singh, S. Theoretical Insights into the Role of Water in the Dissolution of Cellulose Using IL/Water Mixed Solvent Systems. *J. Phys. Chem. B* **2015**, *119*, 14339−14349.
(49) Stange, P.; Fumino, K.; Ludwig, R. Ion Speciation of Protic Ionic Liquids in Water: Transition from Contact to Solvent-Separated Ion Pairs. *Angew. Chem., Int. Ed.* **2013**, *52*, 2990−2994.
(50) Marcus, Y.; Hefter, G. Ion Pairing. *Chem. Rev.* **2006**, *106*, 4585−4621.
(51) Minnick, D. L.; Flores, R. A.; DeStefano, M. R.; Scurto, A. M. Cellulose Solubility in Ionic Liquid Mixtures: Temperature, Cosolvent, and Antisolvent Effects. *J. Phys. Chem. B* **2016**, *120*, 7906−7919.
(52) Ju, Z.; Yu, Y.; Feng, S.; Lei, T.; Zheng, M.; Ding, L.; Yu, M. Theoretical Mechanism on the Cellulose Regeneration from a Cellulose/EmimOAc Mixture in Anti-Solvents. *Materials* **2022**, *15*, 1158.
(53) Parafiniuk, M.; Mitoraj, M. P. Origin of Binding of Ammonia−Borane to Transition-Metal-Based Catalysts: An Insight from the Charge and Energy Decomposition Method ETS-NOCV. *Organometallics* **2013**, *32*, 4103−4113.
(54) Parker, T. M.; Burns, L. A.; Parrish, R. M.; Ryno, A. G.; Sherrill, C. D. Levels of symmetry adapted perturbation theory (SAPT). I. Efficiency and performance for interaction energies. *J. Chem. Phys.* **2014**, *140*, No. 094106.
(55) Turney, J. M.; Simmonett, A. C.; Parrish, R. M.; Hohenstein, E. G.; Evangelista, F. A.; Fermann, J. T.; Mintz, B. J.; Burns, L. A.; Wilke, J. J.; Abrams, M. L.; Russ, N. J.; Leininger, M. L.; Janssen, C. L.; Seidl, E. T.; Allen, W. D.; Schaefer, H. F.; King, R. A.; Valeev, E. F.; Sherrill, C. D.; Crawford, T. D. Psi4: an open-source ab initio electronic structure program. *Wiley Interdiscip. Rev.: Comput. Mol. Sci.* **2012**, *2*, 556−565.
(56) Li, Y.; Liu, X.; Zhang, Y.; Jiang, K.; Wang, J.; Zhang, S. Why Only Ionic Liquids with Unsaturated Heterocyclic Cations Can Dissolve Cellulose: A Simulation Study. *ACS Sustainable Chem. Eng.* **2017**, *5*, 3417−3428.
(57) Li, Y.; Liu, X.; Zhang, S.; Yao, Y.; Yao, X.; Xu, J.; Lu, X. Dissolving process of a cellulose bunch in ionic liquids: a molecular dynamics study. *Phys. Chem. Chem. Phys.* **2015**, *17*, 17894−17905.
(58) Guo, J.; Zhang, D.; Duan, C.; Liu, C. Probing anion−cellulose interactions in imidazolium-based room temperature ionic liquids: a density functional study. *Carbohydr. Res.* **2010**, *345*, 2201−2205.
(59) Guo, J.; Zhang, D.; Liu, C. A theoretical investigation of the interactions between cellulose and 1-butyl-3-methylimidazolium chloride. *J. Theor. Comput. Chem.* **2010**, *09*, 611−624.
(60) Ju, Z.; Yao, X.; Luo, Z.; Cao, M.; Xiao, W. Theoretical studies on the noncovalent interaction of fructose and functionalized ionic liquids. *Carbohydr. Res.* **2020**, *487*, No. 107882.
(61) Popelier, P. L. A. Characterization of a Dihydrogen Bond on the Basis of the Electron Density. *J. Phys. Chem. A* **1998**, *102*, 1873−1878.
(62) Koch, U.; Popelier, P. L. A. Characterization of C-H-O Hydrogen Bonds on the Basis of the Charge Density. *J. Phys. Chem.* **1995**, *99*, 9747−9754.
(63) Lipkowski, P.; Grabowski, S. J.; Robinson, T. L.; Leszczynski, J. Properties of the C-H center dot center dot center dot H dihydrogen bond: An ab initio and topological analysis. *J. Phys. Chem. A* **2004**, *108*, 10865−10872.
(64) Rozas, I.; Alkorta, I.; Elguero, J. Behavior of Ylides Containing N, O, and C Atoms as Hydrogen Bond Acceptors. *J. Am. Chem. Soc.* **2000**, *122*, 11154−11161.
(65) Espinosa, E.; Molins, E.; Lecomte, C. Hydrogen bond strengths revealed by topological analyses of experimentally observed electron densities. *Chem. Phys. Lett.* **1998**, *285*, 170−173.
(66) Lefebvre, C.; Rubez, G.; Khartabil, H.; Boisson, J.-C.; Contreras-Garcáa, J.; Hénon, E. Accurately extracting the signature of intermolecular interactions present in the NCI plot of the reduced density gradient versus electron density. *Phys. Chem. Chem. Phys.* **2017**, *19*, 17928−17936.
(67) Chen, L.; Luo, S.-M.; Huo, C.-M.; Shi, Y.-F.; Feng, J.; Zhu, J.-Y.; Xue, W.; Qiu, X. New insight into lignin aggregation guiding efficient synthesis and functionalization of a lignin nanosphere with excellent performance. *Green Chem.* **2022**, *24*, 285−294.
(68) Lu, T.; Chen, Q. Independent gradient model based on Hirshfeld partition: A new method for visual study of interactions in chemical systems. *J. Comput. Chem.* **2022**, *43*, 539−555.
(69) Dong, K.; Liu, X.; Dong, H.; Zhang, X.; Zhang, S. Multiscale Studies on Ionic Liquids. *Chem. Rev.* **2017**, *117*, 6636−6695.

https://doi.org/10.1021/acsomega.2c04915
ACS Omega 2022, 7, 42170−42180